Sensors and Actuators B 220 (2015) 59–67

Contents lists available at ScienceDirect

Sensors and Actuators B: Chemical

journal homepage: www.elsevier.com/locate/snb

Ultrasensitive and low detection limit of acetone gas sensor based on W-doped NiO hierarchical nanostructure

Chen Wang, Jiangyang Liu, Qiuyue Yang, Peng Sun*, Yuan Gao, Fengmin Liu, Jie Zheng, Geyu Lu*

State Key Laboratory on Integrated Optoelectronics, College of Electronic Science and Engineering, Jilin University, 2699 Qianjin Street, Changchun 130012, People's Republic of China

ARTICLE INFO

Article history:
Received 7 February 2015
Received in revised form 5 May 2015
Accepted 17 May 2015
Available online 27 May 2015

Keywords:
Hydrothermal
W-doped NiO
Hierarchical
Acetone
Gas sensor

ABSTRACT

The pristine and W-doped NiO hierarchical flower-like hollow spheres were prepared by a one-step hydrothermal reaction without template and used to fabricate the gas sensors. Their gas sensing performances and possible sensitive mechanism were investigated. The results indicated that the strategy of doping W into NiO could effectively improve the gas sensing properties. The sensor based on the 4.0 at% W-doped NiO exhibited the optimal gas sensing performance, giving a ppb-level detection limit and an ultra-high response of 198.1 to 100 ppm acetone at 250 °C, which was about 139 times higher than that of the pristine NiO. The significantly enhanced sensing properties to acetone could be attributed to the changes in crystallite size, specific surface area, and hole carrier concentration caused by W doping.

1. Introduction

Resistive gas sensors based on metal oxide semiconductors such as SnO_2 [1,2], ZnO [3,4], TiO_2 [5,6], WO_3 [7–12], In_2O_3 [13,14], α-Fe_2O_3 [15], and NiO [16] occupy the significant positions in the field of gas sensors for monitoring and detecting inflammable, explosive, or toxic gases due to the advantages of low cost, simple operation and portability. Extensive research efforts have been committed to develop high-performance gas sensors with high sensitivity and low detection limit [17]. Specially, design and controllable synthesis of hierarchical and hollow nanostructures can effectively improve the gas sensing properties by increasing surface area and decreasing agglomeration [18]. Although the enhanced gas response through structural and morphological adjustment has been demonstrated in the literatures, just relying on this method is far from enough with the growing requirement of the gas sensing performance. The operating principle of resistive gas sensor is based on the change in the concentration of charge carriers caused by the surface oxygen reaction [19,20]. Therefore, the method of tuning the concentration of charge carriers by aliovalent doping should be a promising approach to improve the gas sensing performance [21–25].

Nickel oxide (NiO), as an important p-type metal oxide semiconductor, is a fascinating material for its broad applications in catalysts [26,27] and gas sensor [28–30] since its outstanding chemical and thermal stabilities, as well as the higher amount of chemisorbed oxygen in NiO than that in other metal oxides [31]. Based on the fact that the properties of the material are strongly dependent on its morphology [32,33], different dimensional and morphological NiO nanostructures [34–40] have been synthesized via various methods. Meanwhile, the study about optimizing the sensing properties of the NiO-based gas sensor by doping method has been developing gradually. Yoon et al. [41] have been demonstrated that the response to 100 ppm ethanol could be enhanced up to 217.86 times via doping NiO nanofibers with Fe^{3+}. Kim et al. [25] also have provided an evidence of enhanced gas responses to toluene and xylene by doping NiO spheres with Cr^{3+}. These results reveal that aliovalent doping is an effective measure to modify NiO material in order to tailor its gas sensing properties. It is well known that tungsten (W), which acts as a donor in NiO, can decrease the hole concentration and leads to the increase in the electrical resistivity of NiO. In this case, we expect that W dopant can affect the gas sensing properties of the NiO-based gas sensors. Furthermore, to our best knowledge, the research on the properties of the gas sensors based on the W-doped NiO nanostructures is rarely reported.

In this work, we demonstrated a one-step hydrothermal method to synthesize the undoped and W-doped NiO hierarchical flower-like hollow spheres. A systematically comparative study on morphologies and gas sensing characteristics between the undoped

* Corresponding authors. Tel.: +86 431 85167808; fax: +86 431 85167808.
E-mail addresses: spmaster2008@163.com (P. Sun), lugy@jlu.edu.cn (G. Lu).

http://dx.doi.org/10.1016/j.snb.2015.05.037
0925-4005/

and W-doped NiO were carried out. The results indicated that the sensor based on the 4.0 at% W-doped NiO showed the best gas sensing properties to acetone with a ppb-level detection limit and an ultra-high gas response, which revealed the feasible strategy of doping W into NiO aiming to improve the gas sensing characteristics of the NiO-based gas sensors.

2. Experimental

2.1. Preparation of the undoped and W-doped NiO hierarchical flower-like hollow spheres

The undoped and W-doped NiO hierarchical flower-like hollow spheres were prepared by a hydrothermal reaction. All the chemical reagents in this experiment were analytical grade (Beijing Chemical Co., Ltd.) and used as received without further purification. $NiCl_2{\cdot}6H_2O$ and WCl_6 were used as nickel and tungsten sources, respectively. In brief, 0.4754 g of $NiCl_2{\cdot}6H_2O$ and appropriate amounts of WCl_6 (the molar ratios of W/Ni were 0.0 at%, 2.0 at%, 4.0 at%, and 6.0 at%, respectively) were dissolved in 15 mL of ethanol under vigorous stirring to form a homogeneous solution. Then, 15 mL of 0.13 M hexamethylenetetramine (HMT) aqueous solution and 2 mL of ethanolamine (EA) were added into above solution. After stirring for 10 min, the solution was transferred into a Teflon-lined stainless steel autoclave and heated at 160 °C for 12 h. After cooling down to room temperature, the resulting precipitates were centrifuged and washed with deionized water and ethanol several times and then dried at 80 °C for 24 h. Finally, the undoped and W-doped NiO hierarchical flower-like hollow spheres were obtained by annealing above precipitates at 450 °C for 1 h in air.

2.2. Characterization

The X-ray diffraction (XRD) patterns were recorded on a Rigaku TTRIII X-ray diffractometer operated at 40 kV and 200 mA using Cu $K\alpha$ radiation with a wavelength of 1.5406 Å. The field emission scanning electron microscopy (FESEM) images were obtained using a JSM-7500F (JEOL) microscope with an operating voltage of 15 kV. Transmission electron microscopy (TEM) and high-resolution TEM images were obtained from a JEM-2200FS (JEOL) transmission electron microscope with an operating voltage of 200 kV. The energy dispersive X-ray spectroscopic (EDS) elemental mapping was investigated by the SEM attachment. The X-ray photoelectron spectroscopy (XPS) measurements were performed with Mg-$K\alpha$ X-ray source (1253.6 eV Specs XR50). The specific surface area was estimated from the Brunauer–Emmett–Teller (BET) measurements by using a Micromeritics Gemini VII apparatus (Surface Area and Porosity System).

2.3. Fabrication and measurement of gas sensor

The synthesized products were mixed with ethanol to form a paste. Then the paste was coated onto an alumina tube (4 mm in length, 1.2 mm in external diameter, and 0.8 mm in internal diameter) to form a thick sensitive film. The details of the sensor fabrication have been described in our previous study [42]. The gas sensing properties of the sensor were measured by a static test system. Firstly, the gas sensors were placed in an airtight chamber (50 L in volume) purged with fresh air. Then a certain volume of target gases was injected into the airtight chamber by a micro injector for the measurement of the sensing performance. The gas response of the sensor was defined as R_g/R_a (p-type gas sensor), namely the ratio of the sensor resistance in target gases (R_g) to that of in fresh air (R_a). The response and recovery times were defined as the time taken to achieve 90% of the total resistance changes after the sensor was exposed to the target gases and fresh air, respectively.

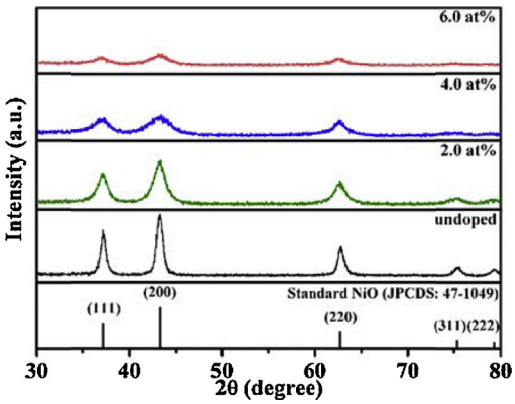

Fig. 1. XRD patterns of the undoped, 2.0 at%, 4.0 at%, and 6.0 at% W-doped NiO samples.

3. Results and discussion

3.1. Structural and morphological characteristics

The XRD patterns of the as-synthesized undoped and W-doped NiO samples are shown in Fig. 1. It is clearly that the diffraction peaks of all samples were matched well with the face-centered cubic phase of NiO (JPCDS Card No. 47-1049). No other peak corresponding to tungsten or tungsten compound was observed in the XRD patterns of the W-doped NiO samples. Besides, the crystallinity of the W-doped NiO samples decreased and the diffraction peaks became broader with increasing the W doping amount. The average crystallite size (D) was calculated according to the Scherrer formula ($D = 0.89\lambda/\beta\cos\theta$, where λ is the X-ray wavelength (0.1518 nm), β is the peak width at half maximum, and θ is the diffraction angle of the peak). The average crystallite sizes of the undoped, 2.0 at%, 4.0 at%, and 6.0 at% W-doped NiO were about 14.2, 11.1, 10.4, and 9.8 nm, respectively. Obviously, the crystallite size also decreased with the increase of the W doping amount. This could be because W prevented NiO nanocrystals from growing-up and combining into larger crystals. These results indicated that W could be incorporated into the lattice of NiO successfully.

The morphological characteristics of the as-synthesized undoped and different W doping amount of NiO are observed by FESEM. It can be clearly seen from the panoramic FESEM image of Fig. 2a that the undoped NiO samples were hierarchical flower-like hollow spheres with good dispersity. Meanwhile, no other morphologies could be observed. A typical single NiO flower-like sphere is observed in Fig. 2b, from which the sphere was assembled by a number of 2D curving nanosheets and showed a diameter of about 4.7 μm. The morphologies of the W-doped NiO products are shown in Fig. 2c–h. Compared with the undoped NiO, the morphologies had some changes. Despite the 2.0 at%, 4.0 at%, and 6.0 at% W-doped NiO samples still maintained hierarchical flower-like hollow spherical morphologies, the nanosheets as the building blocks became much smaller and denser than those of the undoped NiO. Furthermore, with increasing the W doping amount, the sizes of the spheres were also decrease. The observed sizes of the 2.0 at%, 4.0 at%, and 6.0 at% W-doped NiO were about 4.4 μm (Fig. 2d), 3.9 μm (Fig. 2f), and 3.2 μm (Fig. 2h), respectively.

TEM and HRTEM were employed to further investigate the structural features of the W-doped NiO hierarchical flower-like hollow spheres. Fig. 3a shows the TEM image of a single 4.0 at% W-doped NiO hierarchical flower-like hollow sphere. The morphology and size were similar to the FESEM images. Meanwhile, the distinct

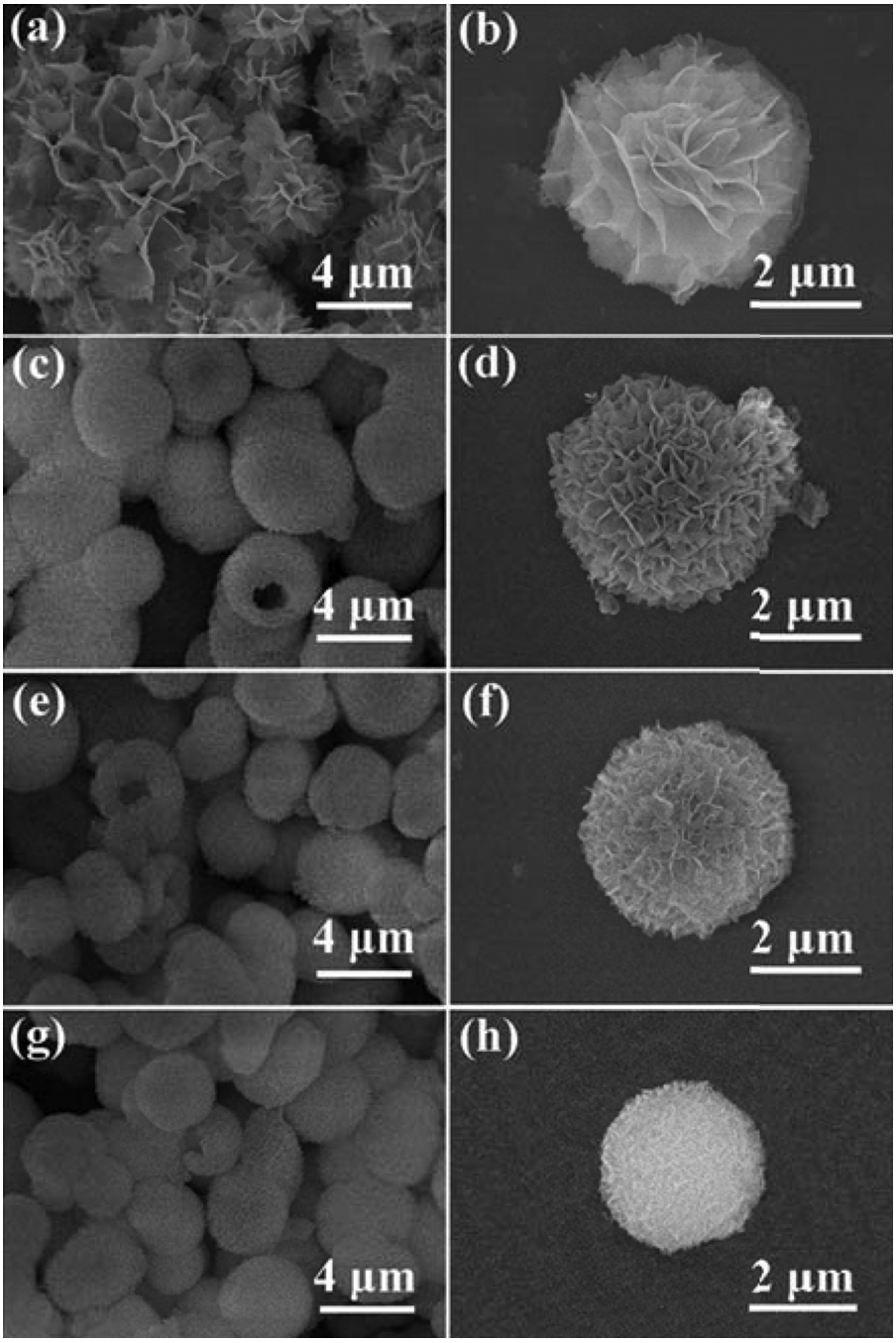

Fig. 2. FESEM images of the undoped (a and b), 2.0 at% (c and d), 4.0 at% (e and f), and 6.0 at% (g and h) W-doped NiO hierarchical flower-like hollow spheres.

hollow spherical structure could be demonstrated according to the obvious constrast between the dark edge and the light region in the center. The high-resolution TEM (HRTEM; Fig. 3b) shows a clear lattice fringe with the lattice spacing of 0.21 nm, corrsponding to the (2 0 0) plane of cubic NiO. The energy dispersive X-ray spectroscopic (EDS) elemental mapping images (Fig. 3c–e) confirms the composition of the product and the spatial distribution of the elements. Obviously, Ni and O signals were detected as a spherical structure, while W signals were detected in the whole spherical region, which indicated the uniform distributions of W element over the whole W-doped NiO hierarchical flower-like hollow spheres.

XPS was also carried out to further investigate the surface compositions and chemical states of the as-synthesized W-doped NiO. Fig. 4a shows the XPS survey spectrum of the 4.0 at% W-doped NiO sample, from which we could clearly observe the peaks of Ni, O, C, and W. The adventitious carbon C 1s peak at 285 eV was used as the reference for calibration the binding energy. Fig. 4b–d show the high resolution scans of Ni 2p, W 4f, and O 1s. The Ni 2p signal could be divided into four peaks (Fig. 4b). The binding energy at 856.6 eV was assigned to the Ni $2p_{3/2}$ peak, and its satellite peak appeared at 862.6 eV. The 874.4 and 880.7 eV peaks were attributed to Ni $2p_{1/2}$, and its satellite. The Ni $2p_{3/2}$ peaks were assigned to Ni^{2+}, while the Ni $2p_{1/2}$ peaks were attributed to Ni^{3+} [43]. The W 4f specturm (Fig. 4c) was composed of two obvious peaks at 36.0 and 37.9 eV, belonging to W $4f_{7/2}$ and W $f_{5/2}$ of WO_3, respectively [9]. The O 1s peak was asymmetric and could be fitted into two components. The binding energy peaks located at 531.2 and 532.9 eV were attributed to lattice oxygen in NiO and chemisorbed oxygen species

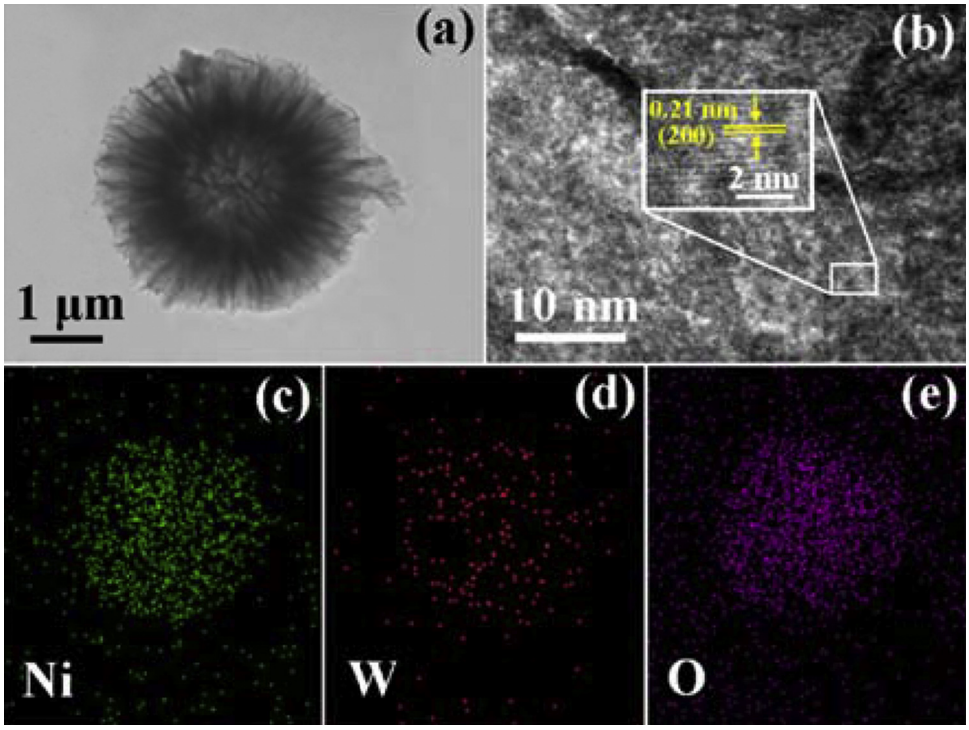

Fig. 3. (a) TEM image of a single 4.0 at% W-doped NiO hierarchical flower-like hollow sphere. (b) The corresponding HRTEM image. (c–e) The corresponding energy dispersive X-ray spectroscopic (EDS) elemental mapping images.

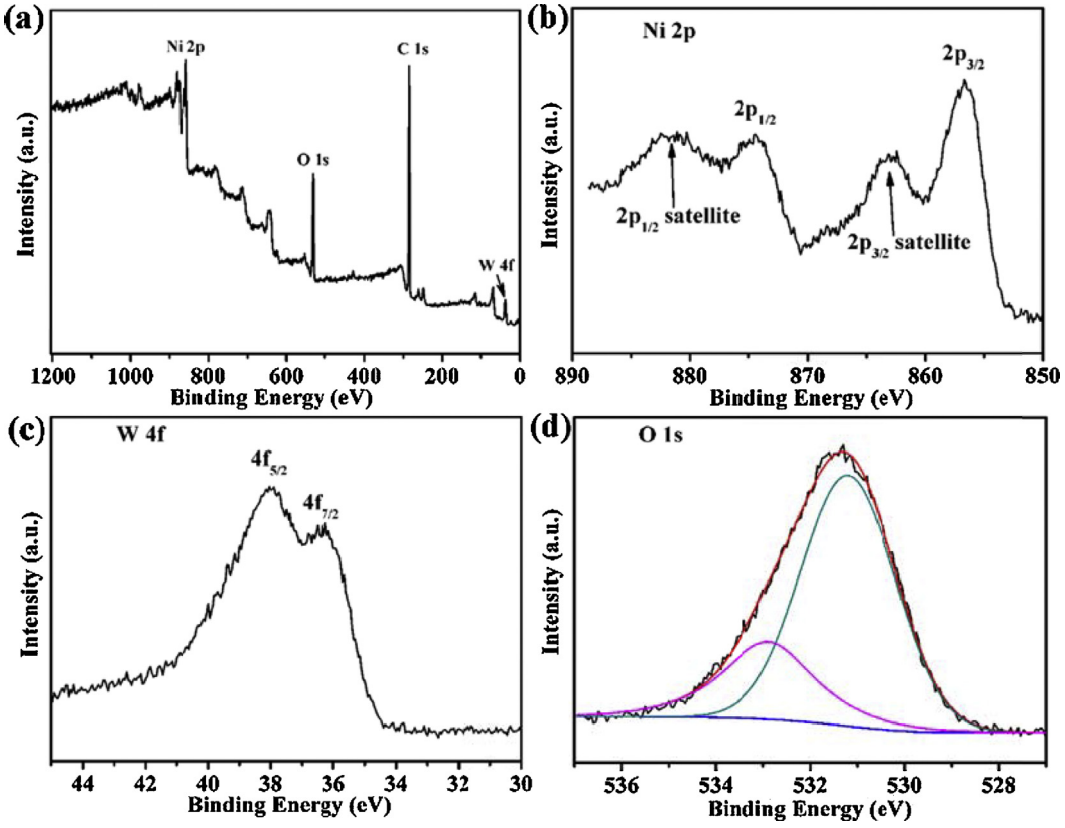

Fig. 4. XPS spectra of the 4.0 at% W-doped NiO hierarchical flower-like hollow spheres: (a) a survey scan, (b) Ni 2p, (c) W 4f and (d) O 1s.

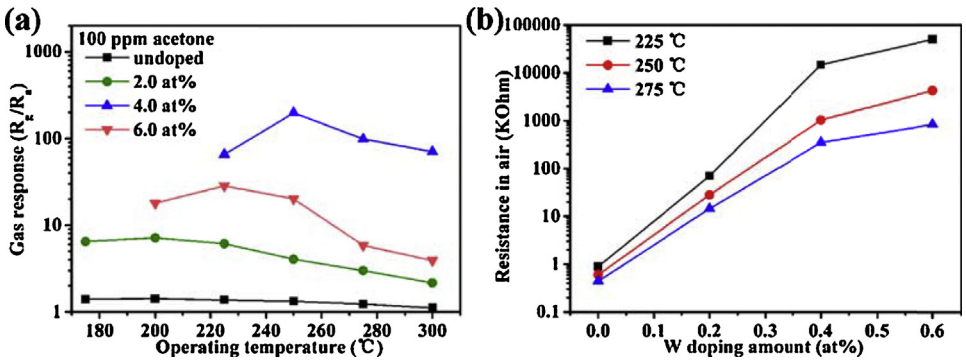

Fig. 5. (a) Responses of the sensors based on the undoped, 2.0 at%, 4.0 at%, and 6.0 at% W-doped NiO hierarchical flower-like hollow spheres as a function of operating temperature to 100 ppm acetone. (b) The dependence of the resistances in air on the doping amount of W for the sensors at various temperatures.

in the surface of NiO, respectively [43]. The above results further confirmed that W^{6+} existed as the phase of WO_3 in the 4.0 at% W-doped NiO sample. In addition, the content of W was 4.07 at%, which was similar to the theoretical value.

3.2. Gas sensing characteristics

The gas sensing properties of the sensors based on the undoped and different W doping amount of NiO were investigated. The operating temperature and the amount of dopant have great influences on the gas sensing properties for metal oxide semiconductor gas sensor. Fig. 5a shows the responses of the gas sensors based on the undoped, 2.0 at%, 4.0 at%, and 6.0 at% W-doped NiO hierarchical flower-like hollow spheres to 100 ppm acetone measured at different operating temperature aiming to determine the optimum operating temperature and the optimum doping amount. It is obvious that the response of all sensors increased with increasing the operating temperature until the value reached maximum at an optimum operating temperature and then decreased with further increasing the operating temperature. The sensor based on the undoped NiO had a very low response to 100 ppm acetone and the maximum response of 1.42 appeared at 200 °C, while the sensors based on the W-doped NiO showed greatly enhanced responses of 7.1, 198.1, and 28.4 for the W doping amounts of 2.0 at%, 4.0 at%, and 6.0 at% at the different optimum operating temperature of 200, 250 and 225 °C, respectively. Obviously, the sensor based on the 4.0 at% W-doped NiO displayed the highest response to 100 ppm acetone, which was nearly 139 times higher than that of the undoped NiO. It can be seen that the response increased with raising the doping ratio of W when the concentration of W dopant was not too high. However, the response decreased when the doping amount became even larger (such as 6.0 at%). This could be attributed to the excessive surface reaction activity caused by over doped W, which decrease the utility factor of the sensing body. Therefore, the doping amount of 4.0 at% was considered as the optimum doping amount and chosen to further investigate the sensing properties. Fig. 5b shows the dependence of the sensor resistance in air (R_a) on the W doping amount for the sensors at various temperatures. It can be observed that the resistances of all sensors decreased with the rise of the operating temperature. Moreover, R_a increased with increasing the W doping amount from 0.0 at% to 6.0 at%. This phenomenon could be explained by the decrease of the hole concentration due to the doping of W [41].

Fig. 6 shows the responses of the sensor based on the 4.0 at% W-doped NiO to 100 ppm various tested gases including acetone, ethanol, methanol, benzene, CO, NH_3, and formaldehyde at different operating temperature. The selectivity of acetone was improved with raising the operating temperature from 200 to 275 °C. The sensor had a higher response to ethanol than that to acetone at the operating temperature of 225 °C. Nevertheless, the response of the sensor to acetone increased and exceeded that to ethanol with the operating temperature over 250 °C. The response of the sensor to 100 ppm acetone was 1.2 times higher than that to ethanol at 250 °C and then increased to 1.5 times at 275 °C.

The responses of three kinds of sensors on exposure to 100 ppm various gases at 250 °C were also tested with the results shown in Fig. 7. It can be verified that the responses to acetone, ethanol, methanol, and benzene were significantly enhanced via doping W into NiO. The sensors based on the undoped, 2.0 at%, and 4.0 at% W-doped NiO all had the highest response to acetone at 250 °C, while

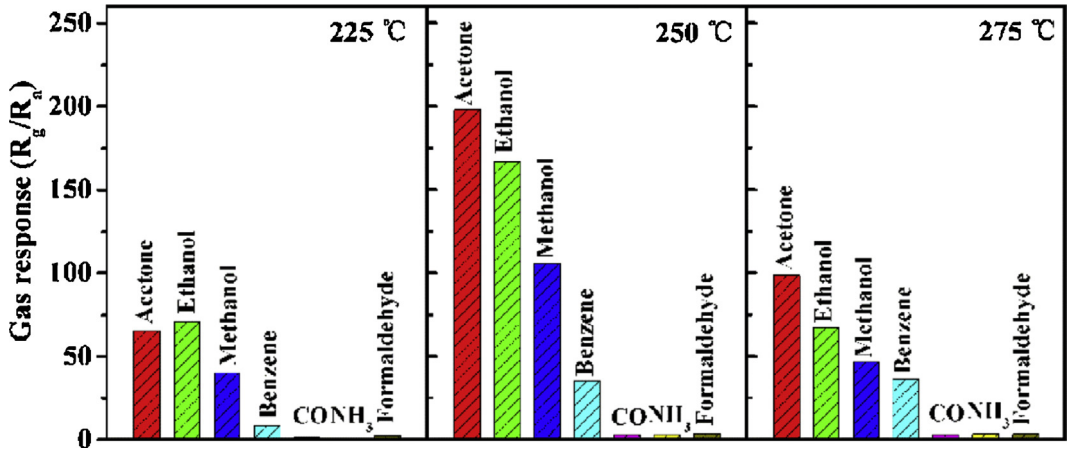

Fig. 6. Responses of the sensor based on the 4.0 at% W-doped NiO hierarchical flower-like hollow spheres to 100 ppm various tested gases at different temperatures.

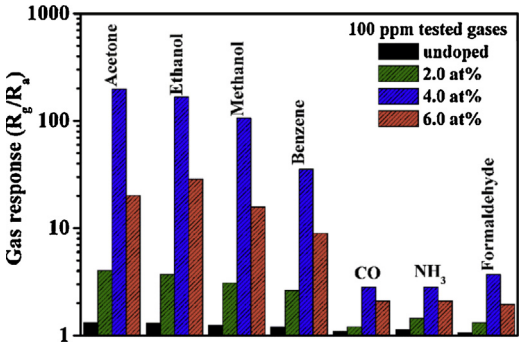

Fig. 7. Responses of the sensors based on the undoped, 2.0 at%, 4.0 at%, and 6.0 at% W-doped NiO hierarchical flower-like hollow spheres to 100 ppm various tested gases at 250 °C.

the sensor based on the 6.0 at% W-doped NiO displayed the best response to ethanol. In addition, the sensor based on the 4.0 at% W-doped NiO present the enhanced response to each tested gas compared with that of the undoped, 2.0 at%, and 6.0 at% W-doped NiO samples. The highest response was about 198.1 to 100 ppm acetone, which was about 1.2–70.2 times higher than those for other tested gases. The results revealed that the sensor based on the 4.0 at% W-doped NiO had a relatively excellent selectivity to acetone. It is well known that the selectivity is closely related to the different reaction activities of the analyte gases to the sensing material [41]. The reaction activities of the analyte gases can be greatly influenced by the operating temperature. Meanwhile, the doping of W can induce the increase of defect in the NiO and thus change the surface reaction activity of the sensing material. Therefore, the selective detection of acetone using W-doped NiO can be realized via the control of the operating temperature and the concentration of W dopant.

The responses of four kinds of sensors as the function of the acetone concentration ranging from 10 to 1000 ppm at 250 °C are depicted in Fig. 8a. Evidently, the response increased with increasing the acetone concentration from 10 to 1000 ppm for all four kinds of sensors, and the growth gradually slowed down. Among them, the response of the sensor based on the 4.0 at% W-doped NiO was apparently higher than those of the undoped, 2.0 at%, and 6.0 at% W-doped NiO to different acetone concentration we tested. Furthermore, according to the gas absorption model of semiconductors, the gas response (S_g) relation to target gas concentration (C_g) can be empirically represented by [44,45]

$$S_g = a\,C_g^{\beta} + 1 \tag{1}$$

where a is a prefactor, and β is the response order. The value of β is usually 1 for the adsorbed surface oxygen ion of O^- or 1/2 for O^{2-}, depending on the charge state of the surface species, the stoichiometry of the elementary surface reactions, and the microstructure of the sensing material. Eq. (1) can be rewritten as

$$\log(S_g - 1) = \log a + \beta\ \log C_g \tag{2}$$

It is clearly that β is the slope value of the log $(S_g - 1) \sim \log C_g$ curve. Fig. 8b depicts a good linear relation between the log $(S_g - 1)$ and log C_g for all four kinds of sensors. The values of β of the sensors based on the undoped, 2.0 at%, 4.0 at%, and 6.0 at% W-doped NiO were 0.283, 0.602, 0.899, and 0.794, respectively. This indicated that the dominant adsorbed oxygen species at the surfaces of the undoped and 2.0 at% W-doped NiO was O^{2-}, while that at the surfaces of the 4.0 at%, and 6.0 at% W-doped NiO was O^- [44,45]. To further demonstrate the excellent gas sensing performance of the sensor based on the 4.0 at% W-doped NiO, the dynamic response and recovery characteristics of the sensor to various acetone concentrations at 250 °C are displayed in Fig. 8c. It is observed that the responses of the sensor were 18.4–834.9 to the acetone concentrations from 10 to 1000 ppm. Meanwhile, the sensor exhibited excellent response and recovery characteristics with respect to different acetone concentrations ranging from 10 to 1000 ppm.

In addition, the gas sensing performance of the sensor based on the 4.0 at% W-doped NiO to low acetone concentrations at 250 °C was further measured and shown in Fig. 9. It is found that the responses were about 2.1, 3.0, 4.0, 4.4, 5.1, 7.7, 9.4, and 13.3 to 0.1, 0.3, 0.5, 0.8, 1, 3, 5, and 8 ppm acetone, respectively. The transient curve showed stable response and recovery characteristics. This indicated that the sensor based on the 4.0 at% W-doped NiO hierarchical flower-like hollow spheres had ppb-level detection limit and thus, had the potential application value in breathing diagnosis for diabetes.

3.3. Mechanism of the enhanced gas sensing performance

For semiconducting metal oxide based resistive gas sensor, the most widely accepted sensing mechanism is the change in the electrical conductivity caused by the interactions between the surface chemisorbed oxygen species and target gases [19,20,46,47]. The electrical conductivity is determined by the charge carrier concentration of the sensing materials, which is a decisive factor for the gas response. NiO is a *p*-type semiconductor with holes as the main species of charge carriers. In the ambient atmosphere, the chemisorption of oxygen leads to an hole accumulation layer via capturing electrons from the valance band of NiO and thus to a lower resistance. When reducing gas (e.g. acetone) is present, the gas molecules will react with chemisorbed oxygen ions. This process releases electrons to NiO and causes the decrease of the accumulation layer thickness, which results in the increase in the sensor resistance.

The enhancement of the gas response of the sensor based on the W-doped NiO hierarchical flower-like hollow spheres are likely to

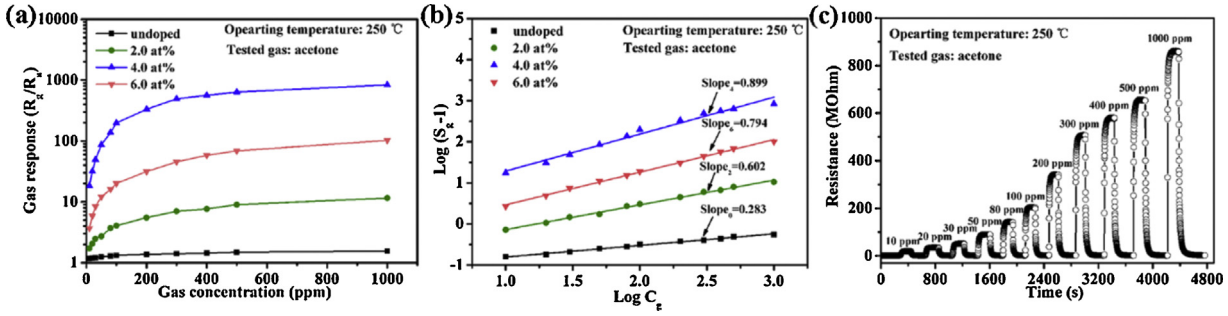

Fig. 8. (a) Responses of the sensors based on the undoped, 2.0 at%, 4.0 at%, and 6.0 at% W-doped NiO hierarchical flower-like hollow spheres versus acetone concentration at 250 °C. (b) Log $(S_g - 1)$ vs log C_g plots of the four sensors. (c) Dynamical response-recovery curves of the sensor based on the 4.0 at% W-doped NiO hierarchical flower-like hollow spheres to different acetone concentrations at 250 °C.

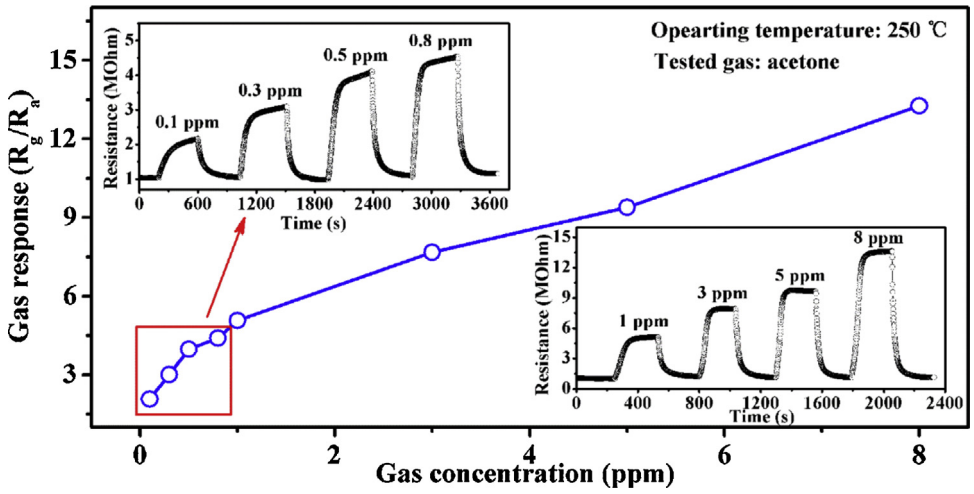

Fig. 9. Response of the sensor based on the 4.0 at% W-doped NiO hierarchical flower-like hollow spheres to low acetone concentrations from 0.1 to 8 ppm at 250 °C.

Table 1
Comparison of the average crystallite sizes and specific surface areas of the undoped, 2.0 at%, 4.0 at%, and 6.0 at% W-doped NiO samples.

Sample name	Undoped NiO	2.0 at% W-doped NiO	4.0 at% W-doped NiO	6.0 at% W-doped NiO
Average crystallite size (nm)	14.2	11.1	10.4	9.8
Specific surface area ($m^2\ g^{-1}$)	117.4	197.8	217.2	44.4

be attribute to the changes in crystallite size, specific surface area, and carrier concentration because of W doping. The comparison of average crystallite sizes and specific surface areas of the undoped, 2.0 at%, 4.0 at%, and 6.0 at% W-doped NiO samples are summarized in Table 1. As previously mentioned, the crystallite size decreases with the increase of the W doping amount. The specific surface areas of the undoped, 2.0 at%, 4.0 at%, and 6.0 at% W-doped NiO samples are about 117.4, 197.8, 217.2, and 44.4 $m^2\ g^{-1}$, respectively (Fig. 10). Apparently, the specific surface area increases greatly with raising the W doping amount when the concentration of W dopant

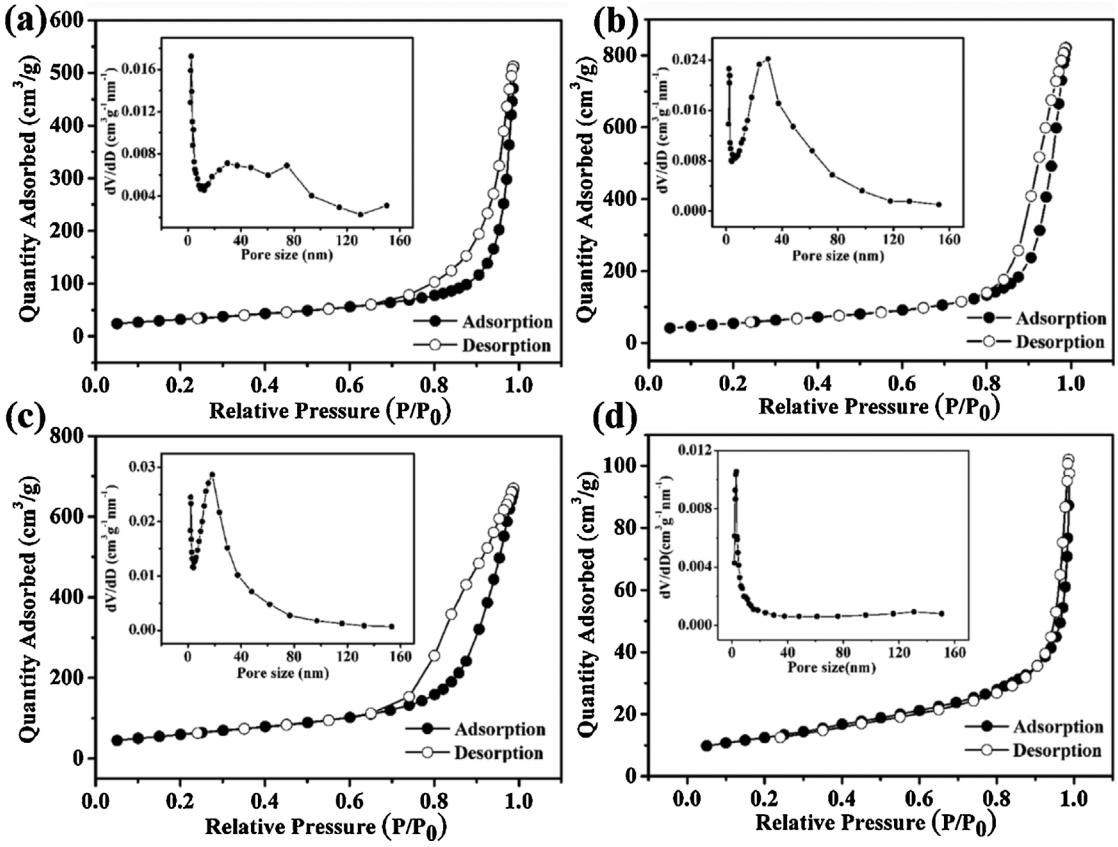

Fig. 10. N_2 adsorption-desorption isotherms of the (a) undoped, (b) 2.0 at%, (c) 4.0 at% and (d) 6.0 at% W-doped NiO samples.

was not too high. This means that the surface activity of the sensing material is significantly improved to make more oxygen can be absorbed and ionized due to W doping. Meanwhile, the diffusion of both the target gas and oxygen to the gas sensing bodies, and the reaction between the target gas molecules and the chemisorbed oxygen ions are also facilitated. However, the decrease of the specific surface area of the 6.0 at% W-doped NiO sample may due to the too dense spherical shell structure of the hierarchical flower-like hollow spheres. Therefore, the enhanced gas responses may be partly explained by the decrease of the crystallite size and the increase of the specific surface area.

The change in carrier concentration may be the key factor for the enhanced gas response. According to the previous research by Kim et al. [24], the gas response can be written as follows:

$$S_g = \frac{R_g}{R_a} = \frac{p_a}{p_g} = \frac{\Delta p}{p_a - \Delta p} + 1 \quad (3)$$

where R_a and R_g are the sensor resistance in air and in target gas, p_a and p_g are the hole concentrations in air and target gas, and $\Delta p = p_a - p_g$ is the variation of the hole concentration on exposure to target gas. Accordingly, a higher variation in the sensor resistance can be got when the hole concentration of p-type oxide semiconductor in air become lower, suggesting that electronic sensitization can be utilized to improve the gas response of p-type oxide semiconductor gas sensor. The substitution of W^{6+} at the site of Ni^{2+} can be compensated by two different charge compensation mechanism (electronic compensation, Eq. (4); ionic compensation, Eq. (5)) as follows:

$$WO_3 \xrightarrow{NiO} W_{Ni}^{\bullet\bullet\bullet\bullet} + 4e' + O_O^{\times} + O_2(g) \quad (4)$$

$$WO_3 \xrightarrow{3NiO} W_{Ni}^{\bullet\bullet\bullet\bullet} + 3O_O^{\times} + 2V_{Ni}'' \quad (5)$$

From the incorporation reaction in Eq. (4), we can reach a conclusion that the sensor resistance will increase with increasing W doping amount, which is consistent with the results in Fig. 5c. Thus, the electronic compensation mechanism is more plausible. In this reaction, electrons are generated to compensate for substituting W^{6+} into Ni^{2+} sites, which decrease the hole concentration in NiO (p_a). As seen in Eq. (3), when the value of p_a become very small, the significantly enhanced response (S_g) can be easily obtained even to very low acetone concentration (i.e. the value of Δp is very small). Therefore, the enhanced gas response of the NiO-based gas sensor can be successfully realized via adjusting the hole concentration using W doping strategy.

4. Conclusion

The undoped and W-doped NiO hierarchical flower-like hollow spheres were successfully synthesized by the facile hydrothermal route and utilized to fabricate promising acetone gas sensor to achieve ultra-high sensitivity and low detection limit. The results of gas sensing measurement indicated that the sensor based on the 4.0 at% W-doped NiO has the significantly enhanced gas response to acetone compared with that of the undoped, 2.0 at%, and 6.0 at% W-doped NiO. The changes in crystallite size, specific surface area, and carrier concentration caused by W doping could be responsible for the improvement of sensing properties.

Acknowledgments

This work is supported by the National Natural Science Foundation of China (Nos. 61374218, 61134010, 61474057, 61304242, 61377058 and 61327804) and Program for Chang Jiang Scholars and Innovative Research Team in University (No. IRT13018). National High-Tech Research and Development Program of China (863 Program, No. 2013AA030902 and 2014AA06A505).

References

[1] P. Sun, X.D. Mei, Y.X. Cai, J. Ma, Y.F. Sun, X.S. Liang, F.M. Liu, G.Y. Lu, Synthesis and gas sensing properties of hierarchical SnO_2 nanostructures, Sens. Actuators, B: Chem. 187 (2013) 301–307.
[2] C.P. Gu, X.J. Xu, J.R. Huang, W.Z. Wang, Y.F. Sun, J.H. Liu, Porous flower-like SnO_2 nanostructures as sensitive gas sensors for volatile organic compounds detection, Sens. Actuators, B: Chem. 174 (2012) 31–38.
[3] H.N. Hieu, N.M. Vuong, H. Jung, D.M. Jang, D. Kim, H. Kim, S.-K. Hong, Optimization of a zinc oxide urchin-like structure for high-performance gas sensing, J. Mater. Chem. 22 (2012) 1127–1134.
[4] D.W. Wang, S.S. Du, X. Zhou, B. Wang, J. Ma, P. Sun, Y.F. Sun, G.Y. Lu, Template-free synthesis and gas sensing properties of hierarchical hollow ZnO microspheres, CrystEngComm 15 (2013) 7438–7442.
[5] H.-Y. Yang, X.-L. Cheng, X.-F. Zhang, Z.-K. Zheng, X.-F. Tang, Y.-M. Xu, S. Gao, H. Zhao, L.-H. Huo, A novel sensor for fast detection of triethylamine based on rutile TiO_2 nanorod arrays, Sens. Actuators, B: Chem. 205 (2014) 322–328.
[6] L.P. Liu, X.G. Li, P.K. Dutta, J. Wang, Room temperature impedance spectroscopy-based sensing of formaldehyde with porous TiO_2 under UV illumination, Sens. Actuators, B: Chem. 185 (2013) 1–9.
[7] J.R. Huang, X.J. Xu, C.P. Gu, M. Yang, M. Yang, J.H. Liu, Large-scale synthesis of hydrated tungsten oxide 3D architectures by a simple chemical solution route and their gas-sensing properties, J. Mater. Chem. 21 (2011) 13283–13289.
[8] C. Wang, R.Z. Sun, X. Li, Y.F. Sun, P. Sun, F.M. Liu, G.Y. Lu, Hierarchical flower-like WO_3 nanostructures and their gas sensing properties, Sens. Actuators, B: Chem. 204 (2014) 224–230.
[9] L. Yin, D.L. Chen, M.X. Hu, H.Y. Shi, D.W. Yang, B.B. Fan, G. Shao, R. Zhang, G.S. Shao, Microwave-assisted growth of In_2O_3 nanoparticles on WO_3 nanoplates to improve H_2S-sensing performance, J. Mater. Chem. A 2 (2014) 18867–18874.
[10] D.L. Chen, L.F. Ge, L. Yin, H.Y. Shi, D.W. Yang, J. Yang, R. Zhang, G.S. Shao, Solvent-regulated solvothermal synthesis and morphology-dependent gas-sensing performance of low-dimensional tungsten oxide nanocrystals, Sens. Actuators, B: Chem. 205 (2014) 391–400.
[11] D.L. Chen, L. Yin, L.F. Ge, B.B. Fan, R. Zhang, J. Sun, G.S. Shao, Low-temperature and highly selective NO-sensing performance of WO_3 nanoplates decorated with silver nanoparticles, Sens. Actuators, B: Chem. 185 (2013) 445–455.
[12] D.L. Chen, X.X. Hou, H.J. Wen, Y. Wang, H.L. Wang, X.J. Li, R. Zhang, H.X. Lu, H.L. Xu, S.K. Guan, J. Sun, L. Gao, The enhanced alcohol-sensing response of ultrathin WO_3 nanoplates, Nanotechnology 21 (2010) 035501–035512.
[13] H.-Y. Lai, T.-H. Chen, C.-H. Chen, Architecture controlled synthesis of flower-like In_2O_3 nanobundles with significantly enhanced ultraviolet scattering and ethanol sensing, CrystEngComm 14 (2012) 5589–5595.
[14] X.X. Xu, X.D. Mei, P.L. Zhao, P. Sun, Y.F. Sun, X.L. Hu, G.Y. Lu, One-step synthesis and gas sensing characteristics of urchin-like In_2O_3, Sens. Actuators, B: Chem. 186 (2013) 61–66.
[15] X. Hu, J.C. Yu, J. Gong, Q. Li, G. Li, α-Fe_2O_3 nanorings prepared by a microwave-assisted hydrothermal process and their sensing properties, Adv. Mater. 19 (2007) 2324–2329.
[16] B. Liu, H.Q. Yang, H. Zhao, L.J. An, L.H. Zhang, R.Y. Shi, L. Wang, L. Bao, Y. Chen, Synthesis and enhanced gas-sensing properties of untralong NiO nanowires assembled with NiO nanocrystals, Sens. Actuators, B: Chem. 156 (2011) 251–262.
[17] I.-D. Kim, A. Rothschild, H.L. Tuller, Advances and new directions in gas sensing devices, Acta Mater. 61 (2013) 974–1000.
[18] J.-H. Lee, Gas sensors using hierarchical and hollow oxide nanostructures: overview, Sens. Actuators, B: Chem. 140 (2009) 319–336.
[19] N. Yamazoe, G. Sakai, K. Shimanoe, Oxide semiconductor gas sensors, Catal. Surv. Asia 7 (2003) 63–75.
[20] Y. Shimizu, M. Egashira, Basic aspects and challenges of semiconductor gas sensors, MRS Bull. 24 (1999) 18–24.
[21] P. Sun, X. Zhou, C. Wang, B. Wang, X.M. Xu, G.Y. Lu, One-step synthesis and gas sensing properties of hierarchical Cd-doped SnO_2 nanostructures, Sens. Actuators, B: Chem. 190 (2014) 32–39.
[22] J.P. Cheng, B.B. Wang, M.G. Zhao, F. Liu, X.B. Zhang, Nickel-doped tin oxide hollow nanofibers prepared by electrospinning for acetone sensing, Sens. Actuators, B: Chem. 190 (2014) 78–85.
[23] J. Zhao, T.L. Yang, Y.P. Liu, Z.Y. Wang, X.W. Li, Y.F. Sun, Y. Du, Y.C. Li, G.Y. Lu, Enhancement of NO_2 gas sensing response based on ordered mesoporous Fe-doped In_2O_3, Sens. Actuators, B: Chem. 191 (2014) 806–812.
[24] H.-J. Kim, K.-I. Choi, K.-M. Kim, C.W. Na, J.-H. Lee, Highly sensitive C_2H_5OH sensors using Fe-doped NiO hollow spheres, Sens. Actuators, B: Chem. 171–172 (2012) 1029–1037.
[25] H.-J. Kim, J.-W. Yoon, K.-I. Choi, H.W. Jang, A. Umar, J.-H. Lee, Ultraselective and sensitive detection of xylene and toluene for monitoring indoor air pollution using Cr-doped NiO hierarchical nanostructures, Nanoscale 5 (2013) 7066–7073.
[26] G.M. Bai, H.X. Dai, J.G. Deng, Y.X. Liu, K.M. Ji, Porous NiO nanoflowers and nanourchins: highly active catalysts for toluene combustion, Catal. Commun. 27 (2012) 148–153.

[27] G.M. Bai, H.X. Dai, J.G. Deng, Y.X. Liu, W.G. Qiu, Z.X. Zhao, X.W. Li, H.G. Yang, The microemulsion preparation and high catalytic performance of mesoporous NiO nanorods and nanocubes for toluene combustion, Chem. Eng. J. 219 (2013) 200–208.
[28] X.F. Song, L. Gao, S. Mathur, Synthesis, characterization, and gas sensing properties of porous nickel oxide nanotubes, J. Phys. Chem. C 115 (2011) 21730–21735.
[29] G.X. Zhu, C.Y. Xi, H. Xu, D. Zheng, Y.J. Liu, X. Xu, X.P. Shen, Hierarchical NiO hollow microspheres assembled from nanosheet-stacked nanoparticles and their application in a gas sensor, RSC Adv. 2 (2012) 4236–4241.
[30] B. Miao, W. Zeng, L.Y. Lin, S. Xu, Characterization and gas-sensing properties of NiO nanowires prepared through hydrothermal method, Physica E: Low-dimension. Syst. Nanostruct. 52 (2013) 40–45.
[31] M. Iwamoto, Y. Yoda, N. Yamazoe, T. Seiyama, Study of metal oxide catalysts by temperature programmed desorption. 4. Oxygen adsorption on various metal oxides, J. Phys. Chem. 82 (1978) 2564–2570.
[32] L.Y. Lin, T.M. Liu, B. Miao, W. Zeng, Synthesis of NiO nanostructures from 1D to 3D and researches of their gas-sensing properties, Mater. Res. Bull. 48 (2013) 449–454.
[33] L. Pan, L. Li, Y.H. Chen, Synthesis of NiO nanomaterials with various morphologies and their electrocatalytic performances for *p*-nitrophenol reduction, J. Sol-Gel Sci. Technol. 62 (2012) 364–369.
[34] Y. Du, W.N. Wang, X.W. Li, J. Zhao, J.M. Ma, Y.P. Liu, G.Y. Lu, Preparation of NiO nanoparticles in microemulsion and its gas sensing performance, Mater. Lett. 68 (2012) 168–170.
[35] B. Liu, H.Q. Yang, H. Zhao, L.J. An, L.H. Zhang, R.Y. Shi, L. Wang, L. Bao, Y. Chen, Synthesis and enhanced gas-sensing properties of ultralong NiO nanowires assembled with NiO nanocrystals, Sens. Actuators, B: Chem. 156 (2011) 251–262.
[36] X. Wan, M. Yuan, S.-L. Tie, S. Lan, Effects of catalyst characters on the photocatalytic activity and process of NiO nanoparticles in the degradation of methylene blue, Appl. Surf. Sci. 277 (2013) 40–46.
[37] W. Zhou, M. Yao, L. Guo, Y.M. Li, J.H. Li, S.H. Yang, Hydrazine-linked convergent self-assembly of sophisticated concave polyhedrons of β-$Ni(OH)_2$ and NiO from nanoplate building blocks, J. Am. Chem. Soc. 131 (2009) 2959–2964.
[38] X. Wang, L.J. Yu, P. Hu, F.L. Yuan, Synthesis of single-crystalline hollow octahedral NiO, Cryst. Growth Des. 7 (2007) 2415–2418.
[39] J. Wang, L.M. Wei, L.Y. Zhang, C.H. Jiang, E.S.-W. Kong, Y.F. Zhang, Preparation of high aspect ratio nickel oxide nanowires and their gas sensing devices with fast response and high sensitivity, J. Mater. Chem. 22 (2012) 8327–8335.
[40] P. Wu, J.H. Sun, Y.Y. Huang, G.F. Gu, D.G. Tong, Solution plasma synthesized nickel oxide nanoflowers: an effective NO_2 sensor, Mater. Lett. 82 (2012) 191–194.
[41] J.-W. Yoon, H.-J. Kim, I.-D. Kim, J.-H. Lee, Electronic sensitization of the response to C_2H_5OH of p-type NiO nanofibles by Fe doping, Nanotechnology 24 (2013) 444005.
[42] C. Wang, X.Y. Cheng, X. Zhou, P. Sun, X.L. Hu, K. Shimanoe, G.Y. Lu, N. Yamazoe, Hierarchical α-Fe_2O_3/NiO composites with a hollow structure for a gas sensor, ACS Appl. Mater. Interfaces 6 (2014) 12031–12037.
[43] B. Zhao, X.-K. Ke, J.-H. Bao, C.-L. Wang, L. Dong, Y.-W. Chen, H.-L. Chen, Synthesis of flower-like NiO and effects of morphology on its catalytic properties, J. Phys. Chem. C 113 (2009) 14440–14447.
[44] Z.H. Wang, J. Xue, D.M. Han, F.B. Gu, Controllable defect redistribution of ZnO nanopyramids with exposed $\{10\bar{1}1\}$ facets for enhanced gas sensing performance, ACS Appl. Mater. Interfaces 7 (2015) 308–317.
[45] F.B. Gu, D. You, Z.H. Wang, D.M. Han, G.S. Guo, Improvement of gas-sensing property by defect engineering in microwave-assisted synthesized 3D ZnO nanostructures, Sens. Actuators, B: Chem. 204 (2014) 342–350.
[46] N. Barsan, C. Simion, T. Heine, S. Pokhrel, U. Weimar, Modeling of sensing and transduction for p-type semiconducting metal oxide based gas sensors, J. Electroceram. 25 (2010) 11–19.
[47] H.-J. Kim, J.-H. Lee, Highly sensitive and selective gas sensors using p-type oxide semiconductors: overview, Sens. Actuators, B: Chem. 192 (2014) 607–627.

Biographies

Chen Wang received the BE degree in Department of Electronic Sciences and Technology in 2013. He is currently working toward the MS degree in the Electronics Science and Engineering department, Jilin University. His research interests include the synthesis of functional materials and their applications in gas sensors.

Jiangyang Liu is graduated from Jilin University of China at the Electronics Science and Engineering department in 2014. The same year, she entered the MS course and majored in microelectronics and solid-state electronics.

Qiuyue Yang is graduated from Jilin University of China at the Electronics Science and Engineering department in 2014. The same year, she entered the MS course and majored in microelectronics and solid-state electronics.

Peng Sun received his PhD degree from the Electronics Science and Engineering department, Jilin University, China in 2014. Now, he is engaged in the synthesis and characterization of the semiconducting functional materials and gas sensors.

Fengmin Liu received the BE degree in Department of Electronic Science and Technology in 2000. She received his Doctor's degree in College of Electronic Science and Engineering at Jilin University in 2005. Now she is a professor in Jilin University, China. Her current research is preparation and application of semiconductor oxide, especial in gas sensor and solar cell.

Yuan Gao received her Doctor's degree in Department of Analytical Chemistry at Jilin University in 2012. Now she is a lecturer in Jilin University, China. Her current research is preparation and application of graphene oxide and semiconductor oxide, especial in gas sensor and biosensor.

Jie Zheng received the BS degree in Physics in 1984 from Northeast Normal University in China and received MS degree and PhD in Condensed Physics in1992 and 2003 respectively from Changchun Institute of Optics, Fine Mechanics and Physics, Chinese Academy of Sciences. His current research interests include the glass optical waveguides and optical fiber devices for optical sensing applications.

Geyu Lu received the BS degree in electronic sciences in 1985 and the MS degree in 1988 from Jilin University in China and the Dr. Eng. degree in 1998 from Kyushu University in Japan. Now he is a professor of Jilin University, China. Presently, he is interested in the development of functional materials and chemical sensors.